LUMINOSITY DISTRIBUTION OF GAMMA-RAY BURST HOST GALAXIES AT REDSHIFT $z = 1$ IN COSMOLOGICAL SMOOTHED PARTICLE HYDRODYNAMIC SIMULATIONS: IMPLICATIONS FOR THE METALLICITY DEPENDENCE OF GRBs

YUU NIINO [1], JUN-HWAN CHOI [2,3], MASAKAZU A. R. KOBAYASHI [4],
KENTARO NAGAMINE [2,5], TOMONORI TOTANI [1] AND BING ZHANG [2]
Draft version November 22, 2010

ABSTRACT

We study the relationship between the metallicity of gamma-ray burst (GRB) progenitors and the probability distribution function (PDF) of GRB host galaxies as a function of luminosity using cosmological hydrodynamic simulations of galaxy formation. We impose a maximum limit to the gas metallicity in which GRBs can occur, and examine how the predicted luminosity PDF of GRB host galaxies changes in the simulation. We perform the Kolmogorov-Smirnov test, and show that the result from our simulation agrees with the observed luminosity PDF of core-collapse supernovae (SNe) host galaxies when we assume that the core-collapse SNe trace star formation. When we assume that GRBs occur only in a low-metallicity environment with $Z \lesssim 0.1 Z_\odot$, GRBs occur in lower luminosity galaxies, and the simulated luminosity PDF becomes quantitatively consistent with the observed one. The observational bias against the host galaxies of optically dark GRBs owing to dust extinction may be another reason for the lower luminosities of GRB host galaxies, but the observed luminosity PDF of GRB host galaxies cannot be reproduced solely by the dust bias in our simulation.

Subject headings: gamma rays: bursts — galaxies: formation — method: numerical

1. INTRODUCTION

Long gamma-ray bursts (GRBs) are the brightest astronomical transient events, and they are important laboratories of high energy astrophysics in extreme conditions, as well as the tools to probe the high-redshift universe. For example, people have used GRBs to estimate the cosmic star formation rate (SFR) density at very high redshifts (e.g., Kistler et al. 2009). The observational association of some of the long GRBs with energetic Type Ic supernovae (SNe, e.g., Hjorth et al. 2003; Stanek et al. 2003) is considered to be the evidence that at least some of the GRBs originate from core-collapses of very massive stars. Zhang et al. (2009) applied multiple criteria to identify GRBs whose progenitors are related to core collapses of massive stars (the so-called "Type II" GRBs), and found that they mostly correspond to the traditional 'long' GRB population. Hereafter 'GRB' means Type II GRBs, and 'SN' means core-collapse SN, unless otherwise stated.

Although GRBs may originate from the core-collapses of very massive stars, the occurrence rate of GRBs is much lower than that of normal SNe, and the conditions required for a GRB to occur from a SN still remain as one of the most outstanding questions in current astrophysics. A better understanding of required conditions for a GRB to occur would constrain the physical mechanisms of GRBs, and allow us to predict the GRB detection rate for the future observations more reliably.

niinou@kusastro.kyoto-u.ac.jp

[1] Department of Astronomy, School of Science, Kyoto University, Sakyo-ku, Kyoto 606-8502, Japan

[2] Department of Physics and Astronomy, University of Nevada, Las Vegas, 4505 S. Maryland Pkwy, Las Vegas, NV 89154-4002, U.S.A.

[3] Department of Physics and Astronomy, University of Kentucky, Lexington, KY 40506-0055, U.S.A.

[4] Optical and Infrared Astronomy Division, National Astronomical Observatory of Japan, Mitaka, Tokyo 181-8588, Japan

[5] Visiting Researcher, Institute for the Physics and Mathematics of the Universe (IPMU), University of Tokyo, 5-1-5 Kashiwanoha, Kashiwa, 277-8583, Japan

Some theoretical studies on the origin of GRBs using stellar evolution models suggest that a low metallicity environment may be a necessary condition for a GRB to occur (e.g., MacFadyen & Woosley 1999; Yoon & Langer 2005; Woosley & Heger 2006). It has also been suggested from the observations that the metallicity distribution of GRB host galaxies at redshift $z < 0.25$ is significantly biased towards low metallicities compared to the expectation when GRBs are unbiased tracers of star formation (Stanek et al. 2006; Modjaz et al. 2008). However, reliable spectroscopic estimates of metallicities are available only for galaxies at low redshifts ($z \lesssim 0.5$; Savaglio et al. 2009) while the majority of GRBs occur at higher redshift.

Furthermore, some observations suggest that the GRB host galaxies are systematically fainter than those of the core-collapse SNe (Le Floc'h et al. 2003; Fruchter et al. 2006, hereafter F06), indicating that the GRBs may preferentially occur in low metallicity environment, because fainter and lower mass galaxies generally have lower metallicities. These interpretations have also been supported by other theoretical studies using the models of galaxy formation and evolution (Nuza et al. 2007; Lapi et al. 2008; Campisi et al. 2009).

It is also reported that the GRB host galaxies at $z > 2$ have larger Lyα equivalent widths compared to general star-forming galaxies at similar redshifts (Jakobsson et al. 2005; Fynbo et al. 2002, 2003), which is possibly a result of the stronger ionizing flux emitted from low-metallicity stellar population in GRB host galaxies (Niino et al. 2009). Although the Lyα emission property of GRB host galaxies could be used as a metallicity indicator in the studies of GRB progenitors, our current understanding of Lyα transfer in the interstellar medium (ISM) is still inadequate to draw a robust conclusion (Niino et al. 2009), and the samples of GRB host galaxies with Lyα detections is currently very small.

The differences between the observed probability distribution functions (PDF) of GRB and SN host galaxies at $z \sim 1$ as a function of luminosity (hereafter 'luminosity PDF') or

size is consistent with the hypothesis that GRBs occur prefer-
entially in low-metallicity environment (F06). However, it is
not straightforward to connect the difference in the luminos-
ity and/or size of host galaxies to the metallicity difference
of GRB and SN progenitors. In fact, some studies of GRB
host properties claim that GRBs can be produced in higher
metallicity environments than suggested by the stellar evo-
lution models (Wolf & Podsiadlowski 2007; Kocevski et al.
2009). However, their results suffer from some uncertainties
(see § 4.2), and more tests are required to establish the con-
nection between the metallicity dependence of GRBs and the
luminosity PDF of GRB host galaxies.

In this paper, we investigate the relationship between the
low metallicity preference of GRBs and the luminosity of
GRB host galaxies at $z \sim 1$, where relatively large sample of
observed GRB/SN host galaxies is available, using cosmolog-
ical hydrodynamic simulations. We compare the predictions
of our simulations with the observations to test if the low
metallicity preference of GRBs predicted by the stellar evo-
lution models is quantitatively consistent with the observed
luminosity PDF of GRB host galaxies. Several studies on
this topic using galaxy formation models have already been
carried out (Nuza et al. 2007; Lapi et al. 2008; Campisi et al.
2009). However, quantitative comparisons between the pre-
dicted luminosity PDF of GRB host galaxies and the observed
luminosity PDF have not been performed yet.

This paper is organized as follows. In § 2, we briefly de-
scribe our simulation code and show some relevant properties
of simulated galaxies, such as the luminosity function (LF),
dust extinction, and luminosity–metallicity relationship. In
§ 3, we describe the modeling of GRB/SN event rate in the
simulated galaxies, and compare the resulting luminosity PDF
of the GRB/SN host galaxies to the observations. In § 4, we
discuss the effect of possible observational bias by the opti-
cally dark GRBs on the luminosity PDF of GRB host galax-
ies. Then we compare our results with previous studies. Our
conclusions are summarized in § 5.

2. NUMERICAL METHOD AND BASIC DATA

2.1. *Simulations and Galaxy Identification*

We use the modified version of the tree-particle-mesh
smoothed particle hydrodynamics (SPH) code GADGET-3
(originally described in Springel 2005). In this code, the
SPH calculation is performed based on the entropy conserva-
tive formulation (Springel & Hernquist 2002). Our conven-
tional code includes radiative cooling by H, He, and metals
(Choi & Nagamine 2009), heating by a uniform UV back-
ground of a modified Haardt & Madau (1996) spectrum, star
formation, supernova feedback, phenomenological model for
galactic winds, and a sub-resolution model of multiphase ISM
and star formation (Springel & Hernquist 2003).

In this paper, we adopt the following fiducial cosmology
which is consistent with the latest WMAP result: $\Omega_m = 0.26$,
$\Omega_\Lambda = 0.74$, $\Omega_b = 0.044$, $h = 0.72$, $n_s = 0.96$, and $\sigma_8 = 0.80$
(Komatsu et al. 2009, 2010). We use two runs with different
box sizes and resolution: N400L34 and N400L100 run. See
Table 1 for the simulation parameters.

We identify galaxies in the simulation at $z = 1.0$ using a
simplified variant of the SUBFIND algorithm (Springel et al.
2001; Choi & Nagamine 2009). In more detail, the code first
computes a smoothed baryonic density field to identify can-
didate galaxies with high density peaks. The full extent of
these galaxies are found by adding gas and star particles to

Run	Box-size	N_p	m_{DM}	m_{gas}	ϵ
N400L34	33.75	2×400^3	3.60×10^7	7.33×10^6	3.375
N400L100	100.0	2×400^3	9.12×10^8	1.91×10^8	6.45

NOTE. — Simulations employed in the present work. The box-size is
given in units of h^{-1}Mpc, N_p is the particle number of dark matter and gas
(hence $\times 2$), m_{DM} and m_{gas} are the masses of dark matter and gas parti-
cles in units of $h^{-1} M_\odot$, respectively, and ϵ is the comoving gravitational
softening length in units of h^{-1}kpc. The value of ϵ is a measure of spatial
resolution.

the galaxies in the order of declining density. If all N_{min} near-
est neighbor particles have lower densities, this group of par-
ticles is considered as a new galaxy. Here, N_{min} is the min-
imum number of gas and star particles that constitute one
isolated galaxies. In this paper we set $N_{min} = 32$. If there
is a denser neighbor, the particle is attached to the galaxy
to which its nearest denser neighbor already belongs to. If
two nearest neighbors belong to different galaxies and one of
them has less than N_{min} particles, then the two galaxies are
merged. If two nearest neighbors belong to different galax-
ies and both of them has more than N_{min} particles, the parti-
cles are attached to the larger galaxy, leaving the other galaxy
intact. In addition, the gas particles in galaxies should be
denser than $0.01\rho_{th}$, where ρ_{th} is the star formation density
threshold (Springel & Hernquist 2003). In the current sim-
ulations, we use the SF threshold density of $n_{th} = 0.6\,cm^{-3}$
(Choi & Nagamine 2010).

2.2. *Distribution of Gas and Stars*

We first examine the distribution of gas and stars in some
simulated galaxies. Figure 1 is an example of a typical faint
GRB host galaxy with $M_{UV} = -19.0$, while Figure 2 is a more
luminous galaxy with $M_{UV} = -20.3$. In the lower panels of
Figures 1 and 2, the distribution of gas with high- and low-
metallicity is shown separately. In both examples, the high-
metallicity gas is concentrated at the center of its host galaxy,
and the low-metallicity gas is distributed more broadly.

It is reported that the observed GRBs are primarily located
in the brightest regions of galaxies compared to SNe (F06),
and the concentration of high-metallicity gas at the center of
galaxies in our simulation may seem to contradict with the
low-metallicity preference of GRBs. However, if the GRBs
occur in the young star clusters that are not heavily enriched
yet (Larsson et al. 2007), then their occurrence in bright re-
gions would be unrelated to metallicity. We also see from this
figure that our simulations do not have adequate resolution to
resolve the disk structure with spiral arms, therefore it is dif-
ficult to discuss the spatial distribution of GRB sites within a
single galaxy using our current cosmological simulations.

2.3. *Dust Extinction Model*

We compute the spectra and luminosities of simulated
galaxies by applying the GALAXEV population synthesis
code (Bruzual & Charlot 2003) to each constituent star par-
ticles and employing a simple model of dust extinction de-
scribed below. To estimate the degree of extinction in each
simulated galaxy, we assume that E_{B-V} is proportional to the
metal mass column density of the ISM: $\sigma_{ISM} \times Z_{ISM}$, where
σ_{ISM} and Z_{ISM} are the gas column density and metallicity
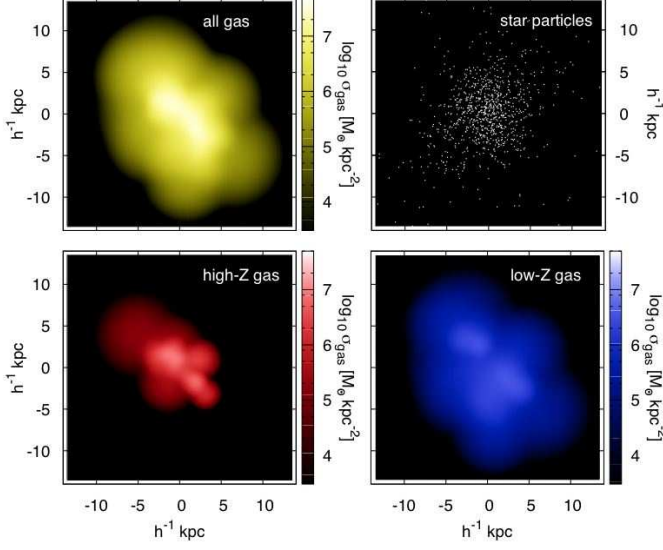of each galaxy, respectively. The proportionality constant

FIG. 1.— Distribution of gas (*top left*) and stars (*top right*) in an example galaxy from the N400L34 run. This galaxy has $M_{UV} = -19.0$, $M_B = -19.3$, $M_\star = 3.5 \times 10^9 M_\odot$, and $Z_{galaxy} = 0.33 Z_\odot$. Distributions of gas with $Z > 2.0 Z_{galaxy}$ and $Z < 0.2 Z_{galaxy}$ are shown in the *bottom left* panel and the *bottom right* panel, respectively.

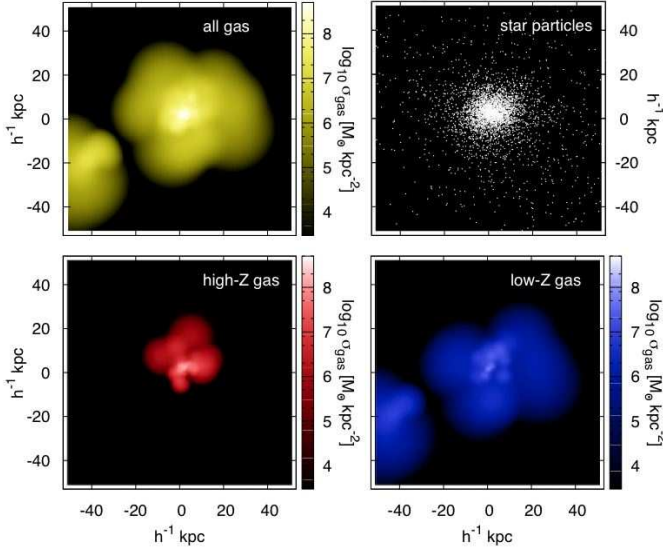FIG. 2.— Same as Fig. 1, but for a more luminous galaxy. This galaxy is from the N400L100 simulation, and has the following properties: $M_{UV} = -20.3$, $M_B = -21.8$, $M_\star = 4.5 \times 10^{11} M_\odot$, and $Z_{galaxy} = 1.2 Z_\odot$.

is fixed so that it agrees with the empirical estimate of gas-to-dust ratio in the Milky Way ($N_H/E_{B-V} = 5.8 \times 10^{21}$ cm^{-2}; Bohlin et al. 1978) when $Z_{ISM} = Z_\odot$:

$$E_{B-V} = \frac{f_H}{5.8 \times 10^{21}} \frac{\sigma_{ISM}}{m_p} \frac{Z_{ISM}}{Z_\odot}, \qquad (1)$$

where $f_H = 0.75$ is the hydrogen mass fraction and m_p is the proton mass. This formulation also agrees with the gas-to-dust ratio in the Small Magellanic Cloud (SMC) $N_H/E_{B-V} \sim 10^{23}$ cm^{-2} (e.g., Bouchet et al. 1985; Fitzpatrick
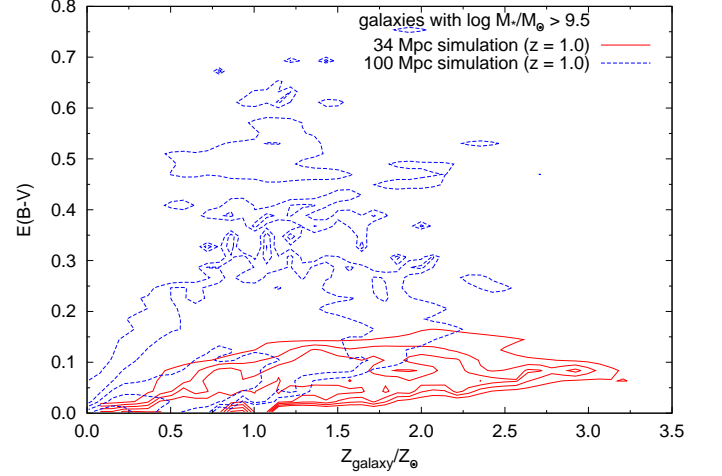

FIG. 3.— Extinction vs. metallicity for the simulated galaxies. The solid (red) and dashed (blue) contours are for the N400L34 and N400L100 runs, respectively. The contours represent $d^3 n_{gal}/dV\,dZ\,dE_{B-V} = 0.01, 0.1, 10, 100,$ and 1000 [h^3Mpc^{-3}mag^{-1}].

1985; Tumlinson et al. 2002), given that the metallicity in SMC is $\sim 10^{-1} Z_\odot$. We use the Calzetti (1997) extinction curve to calculate the extinction at each wavelength.

To estimate σ_{ISM} for each simulated galaxy, we assume that the ISM in each simulated galaxy follows the Hernquist (1990) mass profile with a total gas mass M_{ISM} of the galaxy. Then the mean σ_{ISM} within a radius r is

$$\sigma_{ISM} = \frac{M_{Hernquist}(<r)}{\pi r^2} = \frac{M_{ISM}}{8\pi(r+r_c)^2}, \qquad (2)$$

where the characteristic radius of the Hernquist mass profile r_c is fixed such that $M_{Hernquist}(<l_{smooth,0}) = m_{part,0}$. Here, $l_{smooth,0}$ and $m_{part,0}$ are the SPH smoothing length and the mass of the central gas particle with the highest gas density in the galaxy. For simplicity, we further assume $\sigma_{ISM} = M_{ISM}/8\pi r_c^2$, which gives the value in the central region of the galaxy ($r \ll r_c$), and set Z_{ISM} to the metallicity of the central gas particle, because the highest density region of the galaxy is likely to be the main contributor to both the UV luminosity and GRB/SN production. Note that a single gas particle in our simulation represents a gas mass of $\sim 10^7 - 10^8 M_\odot$, and $l_{smooth,0}$ is typically on the order of kpc.

In Figure 3, we show the distribution of simulated galaxies on the metallicity vs. extinction plane. Note that the metallicity used here is the mean gas metallicity of the whole galaxy (Z_{galaxy}). Only galaxies with $M_\star > 10^{9.5} M_\odot$ are shown in this figure, because the dust extinction in most of the lower mass galaxies are negligible ($E_{B-V} \lesssim 0.01$). The galaxies in the N400L34 run have lower E_{B-V} than those in the N400L100 run for a given metallicity, indicating that σ_{ISM} is lower in the N400L34 run on average. This is consistent with the finding by Choi & Nagamine (2009) that the galaxies with a lower resolution run have higher gas mass fractions, because a higher resolution run can resolve higher density peaks and hence more gas is consumed for star formation.

2.4. *Luminosity Function of Simulated Galaxies*

Figure 4 shows the LFs of simulated galaxies in the N400L100 and N400L34 runs, computed using the GALAXEV population synthesis code (Bruzual & Charlot 2003) and the dust extinction model described in § 2.3.

Each simulation can resolve dark matter halos and galaxies only in a limited mass range due to its limited box-size and resolution. In terms of the galaxy properties, the N400L100 run contains a larger number of massive, brighter galaxies than the N400L34 run due to its larger box size. The N400L34 run can resolve lower-mass, fainter galaxies better than the N400L100 run due to its higher resolution.

The rest-frame B-band LFs are shown in the *top left* panel (dust extinction effect included) of Figure 4 with Poisson error bars. It is clear that the N400L100 run misses the faint galaxies with $M_B \gtrsim -19$, while the volume density of bright galaxies with $M_B \lesssim -20$ in the N400L34 run is smaller than that in the N400L100 run.

Since the two runs probe galaxies with different masses and luminosities, we combine the two LFs by taking the larger of the two runs at each M_B, and compare the result with the observation by Faber et al. (2007) in the *top right* panel of Figure 4. The combined LF agrees quite well with the observation when the dust extinction effect is included.

We also compare the rest-frame UV LF with the observation (Dahlen et al. 2007) in the *bottom* panels of Figure 4. Contrary to the case of rest-frame B-band LF, the discrepancy between the observation and simulation is significant at the bright-end of the rest-frame UV LF. We discuss the effects of this overprediction on our luminosity PDF of GRB host galaxies in § 3.5.

Besides the bright-end overprediction, according to the comparison in Figure 4, the simulation seems to overestimate the galaxy LF at any M_{UV} by a factor of 1.5 at $z = 1.0$. However, this over-estimation is probably within the range of uncertainties in our modeling and the cosmic variance in observations. It should be noted that the vertical shift of LF (e.g., the uniform overprediction at any M_{UV}) does not affect our luminosity PDF of GRB/SN host galaxies.

2.5. *Metallicity of Simulated Galaxies*

The distribution of simulated galaxies on the stellar mass vs. metallicity ($M_\star - Z$) plane is shown in the *left panel* of Figure 5. Here the metallicity means the mean gas metallicity of a galaxy. The N400L34 galaxies are distributed around the empirical formula at $z = 1.0$ proposed by Savaglio et al. (2005), which agrees well with the observational data points by Pérez-Montero et al. (2009). The N400L100 galaxies are distributed on the more massive and luminous side than the N400L34 galaxies as expected from the luminosity functions. In both runs, more massive galaxies have higher metallicities than lower mass galaxies.

We note that the N400L100 galaxies have somewhat lower metallicities on average than those in the N400L34 run for the same $M_\star$. This can be understood as follows. In our simulation, chemical enrichment is calculated as an instantaneous feedback from star formation, and the metallicity of a galaxy increases as the gas is turned into stars. Therefore the metallicity of a galaxy is anti-correlated with the gas mass fraction (f_{gas}) of the galaxy. As mentioned in § 2.3, a higher resolution simulation can consume gas in star formation more efficiently than a lower resolution simulation. Furthermore, if we compare galaxies with similar $M_\star$, galaxies with larger f_{gas} have larger total (star and gas) mass, and thus reside in lager simulation box. The N400L100 run has a higher f_{gas} compared to the N400L34 run due to its larger box size and a lower resolution, leading to a lower metallicity of galaxies. As discussed in § 2.4, the two simulation boxes complement each other, and each of the simulation cannot reproduce the obser-

vations alone for a wide dynamic range. If we combine the two distributions of galaxies shown in the *left panel* of Figure 5, the overall distribution of the simulated galaxies agrees with the observations.

It should be noted that the mean gas metallicity (Z_{galaxy}) of a simulated galaxy depends on the threshold density of gas particles to be included in galaxies, which is a parameter in the galaxy finding algorithm described in § 2.1. If we include lower density gas particles than the current density threshold, each simulated galaxy may have lower Z_{galaxy}, because gas particles in the outskirts of a galaxy have lower metallicity than those near the center (see § 2.2). However, the dependence of Z_{galaxy} on the grouping density threshold does not affect our luminosity PDF of GRB/SN host galaxies. Low density gas particles are not forming stars, and hence they do not contribute to the GRB production and UV luminosity.

The distribution of the simulated galaxies on the $L_{UV} - Z$ plane is also shown in the right panel of Figure 5, which is very similar to the $M_\star - Z$ distribution.

3. RESULTS

3.1. *Metallicity of GRB Sites*

In this section, we explore the metallicity of GRB sites. We first assume that the GRB occurrence rate in each simulated galaxy is proportional to the total SFR without a metallicity limit. Then we examine the models in which the GRB rate is proportional to the total SFR in gas particles with $Z < Z_{crit}$. Our interest is in the luminosity PDF of GRB/SN host galaxies, therefore we do not need to consider the absolute value of the event rate density.

In order to investigate the effect of metallicity limit, we first examine the SFR-weighted distribution of gas particles as a function of metallicity. In Figure 6, we divide the galaxy population into three different samples according to the mean gas metallicity of the host galaxy (Z_{galaxy}). We can see that the metallicity of star forming gas particles has a wider range than that of Z_{galaxy}, showing the large dispersion of gas metallicity in each galaxy. We note that the high metallicity gas is concentrated in the high density regions of its host galaxy (see § 2.2) where SFR is high. Therefore the peak metallicity of SFR-weighted distribution is higher than the mean Z_{galaxy} of the sample. The distributions for both N400L34 and N400L100 runs are very similar to each other.

Assuming that the GRB rate is proportional to the sum of SFR in gas particles with $Z < Z_{crit}$, we can see in Figure 6 that, if we set $Z_{crit} = 0.1 Z_\odot$, then the GRB event rate in galaxies with $Z_{galaxy} \sim 1.0 Z_\odot$ ($0.1 Z_\odot$) would be reduced to a few percent (40%) compared to the case of no Z_{crit}. With $Z_{crit} = 0.1 Z_\odot$, the event rate in galaxies with $Z_{galaxy} \sim 0.01 Z_\odot$ would be almost unchanged from the case of no Z_{crit}. The large fluctuation in the distribution for galaxies with $Z_{galaxy} \sim 0.01 Z_\odot$ is due to the small number of gas particles included in such low-metallicity galaxies.

3.2. *Rest-frame UV Luminosity of the Host Galaxies*

Next, in order to discuss the luminosity PDF of host galaxies, we consider the SFR-weighted fraction of galaxies as a function of rest-frame UV luminosity as shown in Figure 7. The luminosity PDF in the case of no Z_{crit} is plotted in *panel (a)* for the N400L34 and N400L100 runs. As mentioned in § 2.4, the two simulations have different resolving power of galaxies with different mass scales, therefore we combine the two distributions by taking the larger of the two runs in units
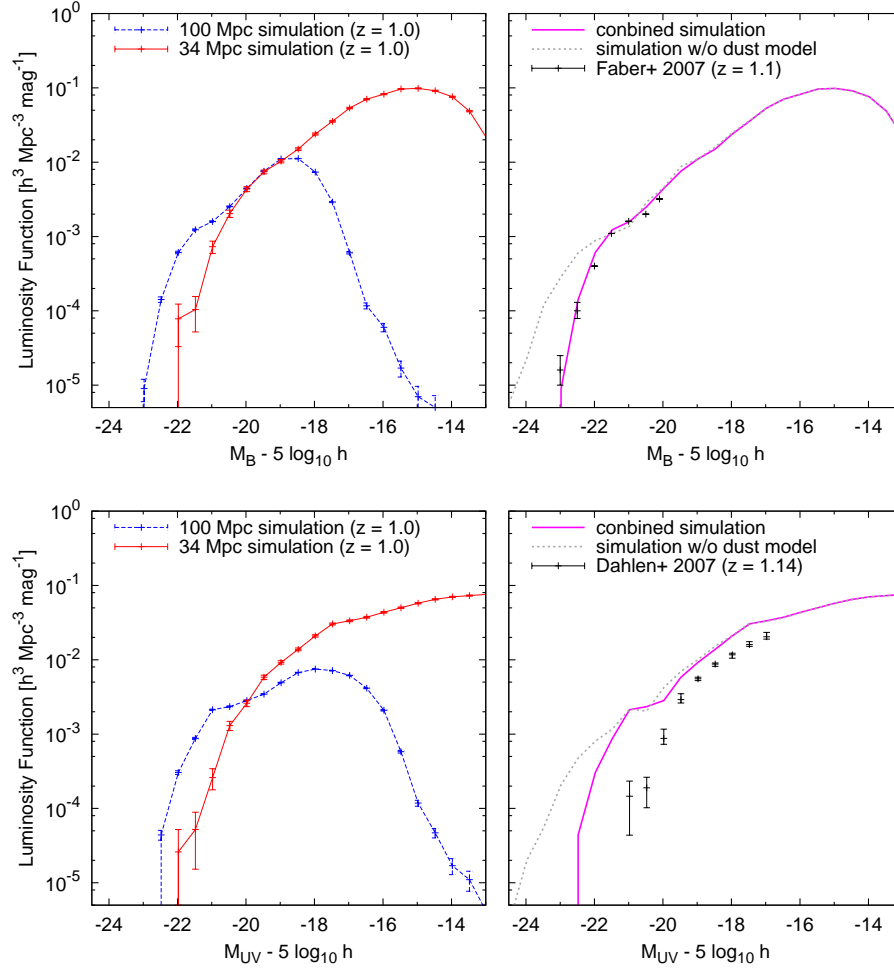
FIG. 4.— Luminosity functions of the simulated galaxies in the rest-frame B-band (*top panels*) and the rest-frame UV (2800 Å, *bottom panels*). *Top left panel*: The solid (red) and dashed (blue) lines are for the N400L34 and N400L100 runs, respectively. The error bars show the Poisson errors. *Top right panel*: The solid (magenta) line represents the combined LF of both the N400L34 and N400L100 runs (i.e., the larger of the two simulation at each magnitude). The LF without dust extinction (i.e., $E_{B-V} = 0$ for all galaxies) is shown with the dotted (grey) line. The same line types are used in the *bottom panels* (rest-frame UV). The observed data points are taken from the DEEP2 survey for B-band (Faber et al. 2007), and the GOODS-S for the UV (Dahlen et al. 2007).

of $M_\odot$ yr^{-1} h^3 Mpc^{-3} mag^{-1} as shown in *panel (a)*. The distributions are normalized so that the integration of the combined luminosity PDF for each Z_{crit} is unity. Hereafter we discuss the combined luminosity PDFs unless otherwise mentioned.

In *panel (b)* of Figure 7, the three combined luminosity PDFs of the simulated host galaxies with Z_{crit} = none, $0.5Z_\odot$, and $0.1Z_\odot$ are shown. The luminosity PDF shifts to the fainter magnitudes as Z_{crit} becomes lower. In the case of $Z_{crit} = 0.1Z_\odot$, the host galaxies are fainter than in the no-Z_{crit} case by ~ 1 magnitude. This result is consistent with the luminosity PDFs of the observed GRB/SN host galaxies at $z < 1.2$ (the F06 sample) as shown in *panel (c)*. The redshift criterion of $z < 1.2$ was proposed in F06 to reduce the effect of galaxy evolution on the comparison between the GRB and SN host galaxies. The luminosity PDF of F06 was in the observed frame V-band, which is close to the UV in the galaxy's rest-frame. The median values of each distribution in *panels (b)* and *(c)* are indicated by the arrows.

It should be noted that, using a larger observed sample, Svensson et al. (2010) found a smaller difference between the GRB and SN host galaxy luminosity PDFs than that claimed by F06. However, it is difficult to understand the selection

effect in the GRB host sample of Svensson et al. (2010), because a part of it is drawn from the GHostS project database, which consists of publicly available data of GRB host observations done by various groups with differing instruments (Savaglio et al. 2009). On the other hand, the F06 sample is a complete sample of host galaxies for all 42 GRBs that have optical afterglow detections ($> 3\sigma$), therefore the sampling effect would be smaller in the F06 sample than in the Svensson et al. (2010) sample. Thus we use the GRB host galaxy sample by F06 as a reference data for the discussions in this paper. The 24 out of the 42 GRBs in the F06 sample are at $z < 1.2$. We note that the SN host galaxies in the Svensson et al. (2010) sample is significantly fainter than those in the F06 sample, and this is probably one of the causes for the smaller difference between the GRB and SN host galaxies. But the reason for the difference between the SN host samples of F06 and Svensson et al. (2010) is not known.

Even the F06 sample would suffer from the observational bias against dusty host galaxies. We will discuss the selection effect caused by the dust extinction in § 4.1.1. We note that the luminosity PDFs studied by F06 and Svensson et al. (2010)
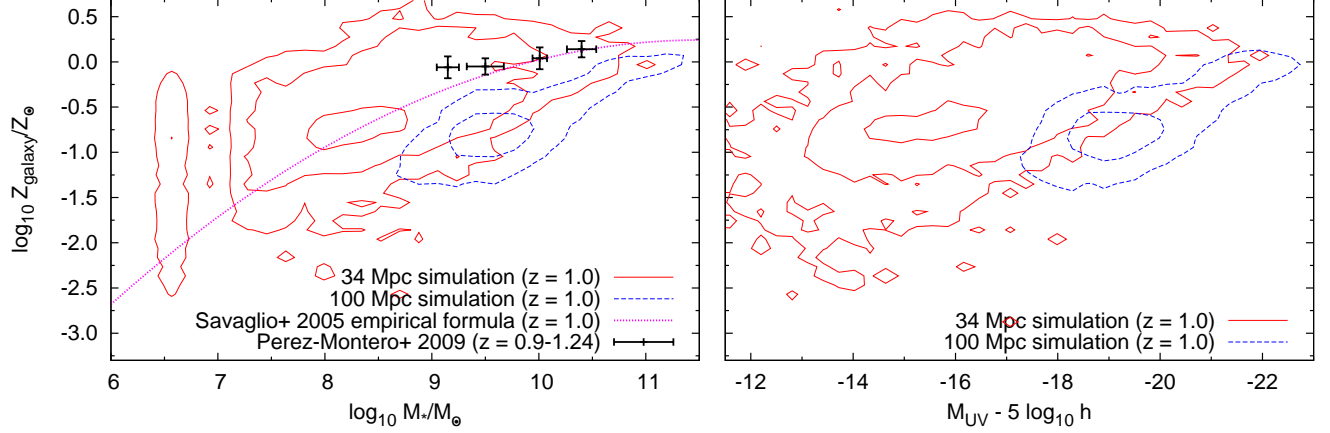
FIG. 5.— *Left:* Distribution of galaxies on $M_\star - Z$ plane. The galaxies in the N400L34 and N400L100 runs are shown with the solid (red) and dashed (blue) contours, respectively. The contours represent $d^3 n_{gal}/dV d(\log_{10} M_\star) d(\log_{10} Z) = 0.005, 0.05,$ and 0.5 $[h^3$ Mpc$^{-3}]$. The stellar mass and metallicity of the observed galaxies at $z \sim 1.0$ (Pérez-Montero et al. 2009) and the empirical formula of Savaglio et al. (2005) for $z = 1.0$ galaxies are plotted together. The empirical formula of Savaglio et al. (2005) is based on the local and $z = 0.7$ galaxies with a mass range of $M_\star \sim 10^{8.5}$–$10^{11} M_\odot$. *Right:* Same as the left panel, but on the M_{UV}-Z plane, where M_{UV} is the restframe UV magnitude. The contours represent $d^3 n_{gal}/dV dM_{UV} d(\log_{10} Z) = 0.002, 0.02,$ and 0.2 $[h^3$ Mpc^{-3} mag$^{-1}]$. Colors are only for the online version.
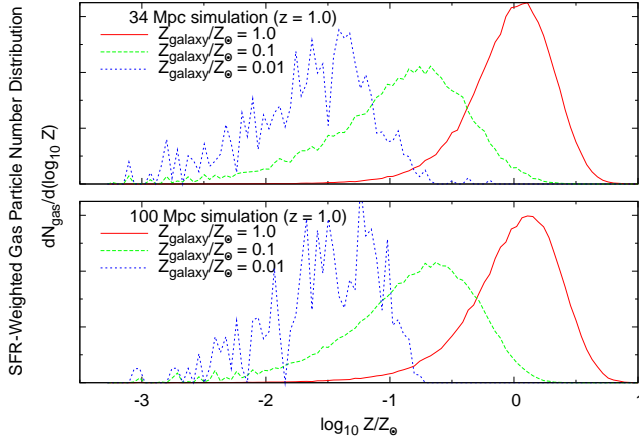

FIG. 6.— SFR-weighted metallicity distributions of gas particles in the simulated galaxies with $\log_{10}(Z_{galaxy}/Z_\odot) = 0.0 \pm 0.15$, -1.0 ± 0.15, and -2.0 ± 0.15 are plotted with solid (red), dashed (green), and dotted (blue) lines, respectively. In our model, we assume that the GRB rate is proportional to the sum of SFR for the gas particles with $Z < Z_{crit}$. The top and bottom panels are showing the distributions for the N400L34 and N400L100 simulations. The large fluctuation in the particle metallicity distribution in galaxies with $Z_{galaxy} = 0.01 Z_\odot$ (blue dotted line) is due to the small number of gas particles included in such low-metallicity galaxies. Colors are only for the online version.

are at different wavelengths [rest-frame UV for F06 versus rest-frame B & V-band for Svensson et al. (2010)], though this cannot explain the difference in their results. The difference in the luminosity PDFs of GRB and SN host galaxies should be larger in the optical than in UV, given that many of observed GRB host galaxies are extremely blue (e.g., Le Floc'h et al. 2003).

3.3. *Cumulative Luminosity PDF*

We plot the cumulative luminosity PDFs of the simulated and observed host galaxies in Figure 8. The simulated PDFs are shown for the cases of $Z_{crit}/Z_\odot$ = none, 0.5, 0.1, 0.025, & 0.001 (top to bottom). The observed host galaxy sample

at $z < 1.2$ of F06 is plotted together as histograms. The shift of luminosity PDF to fainter magnitudes is clearly seen also in the cumulative plot, reproducing the difference in the observed GRB and SN-host galaxy luminosity PDFs. However, the distribution for no-Z_{crit} case overpredicts the bright-end of the observed SN-host luminosity PDFs, and the $Z_{crit} \leq 0.1 Z_\odot$ case overpredicts the bright-end of the observed distribution of GRB host galaxies. This is expected from the overprediction of the UV LF at the bright-end as we discussed in § 2.4 (see the bottom panel of Fig. 4). We discuss the effects of this overprediction on our conclusion in § 3.5.

3.4. *Kolmogorov-Smirnov Test*

To examine the consistency between the simulated and observed cumulative luminosity PDFs shown in Figure 8, we employ the one-sample Kolmogorov-Smirnov (K-S) test, which calculates the probability that a sample distribution is consistent with a given PDF. Here, the sample is the observed luminosity of GRB/SN host galaxies, and the PDFs are the results of our simulation. Figure 9 shows the K-S probability P_{KS} (i.e., one minus the rejection confidence level for consistency) as a function of Z_{crit} of simulated host galaxies. The P_{KS} takes a value between 0 and 1, and $P_{KS} < 10^{-4}$ means that the observed sample is dissimilar to the simulated one at a 3σ level, while a larger P_{KS} means a higher probability that the observed sample is derived from a PDF calculated in our simulation. For the SN host galaxies, we find $P_{KS} > 0.05$ when $Z_{crit} \geq 0.03 Z_\odot$, and $P_{KS} > 0.2$ when $Z_{crit} \geq 0.5 Z_\odot$. On the other hand, for the GRB host galaxies, we find $P_{KS} > 0.05$ (0.2) when $Z_{crit}/Z_\odot \leq 0.1$ (0.03). The KS probabilities are the highest when $Z_{crit}/Z_\odot = 0.005$ and 0.5 for the GRB and SN host galaxies, respectively. This clearly supports the low-metallicity preference for GRB host galaxies.

The luminosity PDF of the simulated host galaxies does not change significantly for $Z_{crit} \leq 0.1 Z_\odot$, and the agreement with the observed PDF is reasonably good for all Z_{crit} values for $Z_{crit} < 0.1 Z_\odot$. Therefore we cannot put a lower limit to Z_{crit} based on this comparison. However our simulation cannot
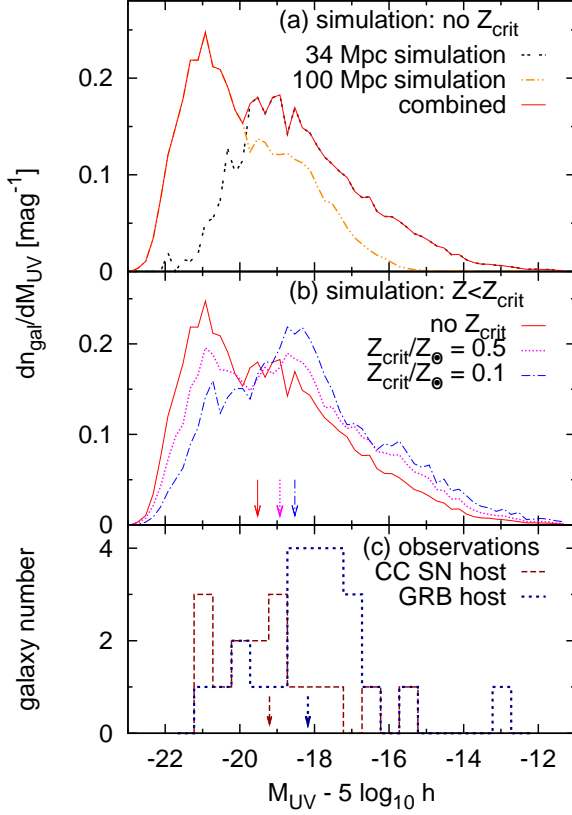
FIG. 7.— (a) Luminosity PDF of the simulated host galaxies ($z = 1.0$) without any metallicity cutoff. The results of the N400L34 and N400L100 run are plotted with double-dotted (black) and double-dot dashed line (orange), respectively. The combined distribution of the two simulations (i.e., the larger of the two distributions) is plotted with solid line (red). (b) Combined luminosity PDFs of the simulated host galaxies with no Z_{crit}, $Z_{crit}/Z_\odot = 0.5$, and 0.1 are plotted with the solid (red), dotted (magenta), and dot-dashed line (blue), respectively. (c) Luminosity PDFs of the observed sample of GRB host galaxies and SN host galaxies at $z < 1.2$ (F06) are plotted with dotted (dark blue) and dashed (dark red) histograms, respectively. The arrows indicate the median of the distributions. Colors are only for online version.
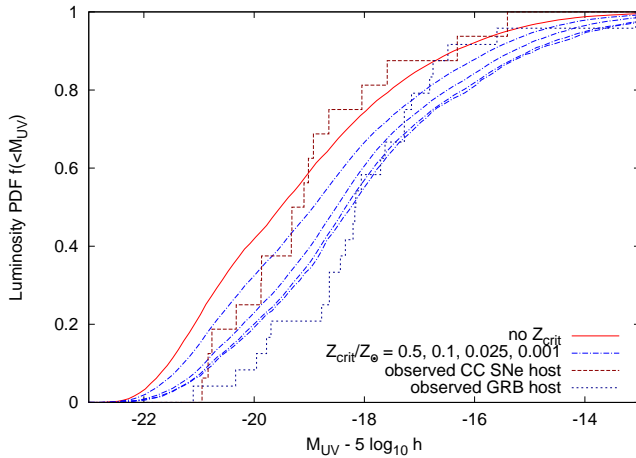

FIG. 8.— Cumulative luminosity PDFs of the simulated host galaxies is shown together with those of the observed GRB/SN host galaxies of F06 at $z < 1.2$, based on the histograms shown in Fig. 7. The PDF without a metallicity cutoff (no Z_{crit}) is shown with the solid line (red), and the those with $Z_{crit}/Z_\odot = 0.5$, 0.1, 0.025, and 0.001 are represented by the dot-dashed lines (blue) from top to bottom, respectively. Colors are only for online version.
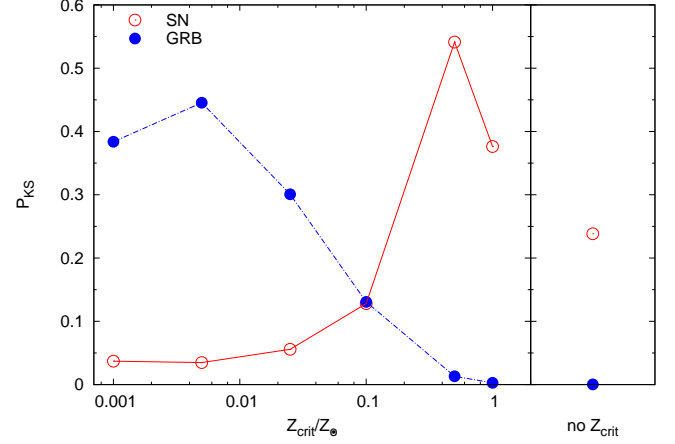

FIG. 9.— K-S probabilities (i.e., 1.0 minus the rejection confidence level for consistency) of the luminosity PDFs of the observed and the simulated host galaxies is plotted against Z_{crit}. The symbols are for the SN host galaxies (red empty circles) and GRB host galaxies (blue filled circles).

resolve the galaxies with $M_\star < 10^8 M_\odot$, therefore it is possible that the above result suffers from the resolution limit of our simulation. We should be cautious about the results with $Z_{crit} < 0.1 Z_\odot$, but our simulation contains galaxies as faint as $M_{UV} \sim -14$ (see the bottom panels of Figure 4), which are well below the typical luminosity of the simulated host galaxies with $Z_{crit} < 0.1 Z_\odot$.

3.5. Overprediction of UV-bright Galaxies

In § 2.4 and Figure 4, we showed that our N400L100 simulation overpredicts the bright-end of the rest-frame UV LF even after the dust extinction correction. We note however that our simulation agrees very well with the observed rest-frame B-band LF, which suggests that either our simulation overpredicts the amount of young stars compared to the older stellar population, or the two sets of observations are inconsistent with each other, or else the Calzetti extinction curve that we adopted is not appropriate for the observed galaxies. The source of this discrepancy is unclear, therefore we focus only on the rest-frame UV LF in this subsection.

To quantify the effect of the bright-end overprediction on our luminosity PDFs, we perform the same K-S test for the following two different test models that modify the shape of the rest-frame UV LF by hand.

- **Model 1**: We double the gradient of the rest-frame UV LF at the bright-end ($M_{UV} < -20$) as follows:

$$M_{UV,\text{model 1}} = M_{UV} + \Delta M_{UV}$$
$$\Delta M_{UV} = \begin{cases} -0.5 \times (M_{UV} + 20), & M_{UV} < -20 \\ 0, & M_{UV} \geq -20. \end{cases} \quad (3)$$

The SFR in galaxies with $M_{UV} < -20$ is also modified in a consistent manner, motivated by the inference that the overprediction of the bright-end of the UV LF is caused by an overestimation of SFR in massive galaxies (e.g., due to lack of active galactic nucleus feedback in our simulation; Choi & Nagamine 2010). The change of SFR in each simulated galaxy is as follows:

$$\Delta(\log_{10} \text{SFR}) = \Delta(\log_{10} L_{UV}) = -\frac{\Delta M_{UV}}{2.5}. \quad (4)$$

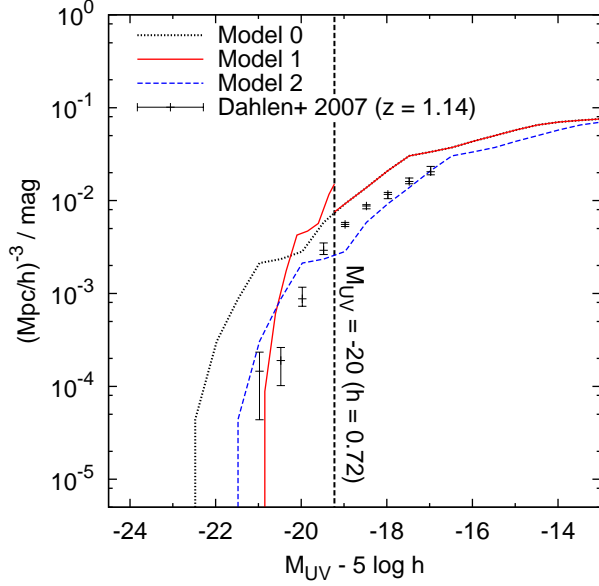- **Model 2**: We shift the entire UV LF uniformly by

FIG. 10.— Rest-frame UV luminosity functions of the simulated galaxies in Model 0, 1 & 2 are plotted together with the observation (Dahlen et al. 2007). The dust extinction model is included. The original result of our simulation (Model 0, identical to the combined simulation shown in the *bottom right panel* of Fig. 4) is shown with the dotted (black) line. The modified LF with the doubled gradient of the bright-end slope (Model 1) and the horizontally shifted LF by $\Delta M_{UV} = 1.0$ (Model 2) are represented by solid (red) and dashed (blue) curves, respectively. Vertical dashed line represents $M_{UV} = -20$, which is the threshold of the bright-end modification in Model 1.

$\Delta M_{UV} = 1.0$ to fit the observation. In this model, the luminosity PDF will also shift by the same amount of ΔM_{UV}, without changing its shape.

Both of these models are ad hoc modifications to fit the observed data points, but they would allow us to evaluate the effects of overprediction of UV LF by our simulation. For comparison purposes, we call the earlier calculations presented in § 3.3 – 3.4 the **Model 0**. We show the LFs of Model 0, 1 & 2 galaxies in Figure 10. One sees that the overprediction of the bright-end in Model 0 is removed in Model 1 & 2. The uniform overprediction at any M_{UV} is not removed in Model 1, but the uniform overprediction does not affect the luminosity PDF of GRB/SN host galaxies, as we have mentioned in § 2.4.

Figure 11 shows the K-S probabilities of Models 1 & 2 for the observed GRB/SN host galaxies. For the SN host galaxies, the no-Z_{crit} case has the highest P_{KS}, and P_{KS} decreases with decreasing Z_{crit}. For the GRB host galaxies, the Model 1 gives the highest probability of $P_{KS} \sim 0.6$ at $Z_{crit} = 0.1 Z_{\odot}$, and $P_{KS} \approx 0.3 - 0.4$ at $Z_{crit} < 0.1 Z_{\odot}$. In the case of Model 2, the trend is opposite of what we saw in Figure 9 for $Z_{crit} < 0.5 Z_{\odot}$ in the sense that P_{KS} increases with increasing Z_{crit}. But the Model 2 still prefers $Z_{crit} = 0.5 Z_{\odot}$ to the no-Z_{crit} case. The Model 2 gives $P_{KS} < 0.2$ across all Z_{crit} values for the SN host galaxies, which means that it doesn't agree well with the observations of SN host galaxies compared to the Models 0 and 1.

4. DISCUSSIONS

4.1. *Effect of Dust Extinction in the Host Galaxies*

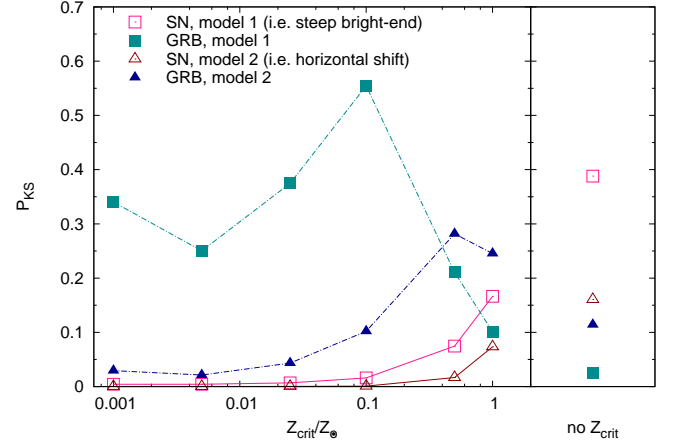#### 4.1.1. *Observational bias against dusty host galaxies*

FIG. 11.— Same as Fig. 9, but for the two different models of modified UV LF (Model 1 & 2). The Model 1 & 2 are represented by the squares and triangles, respectively.
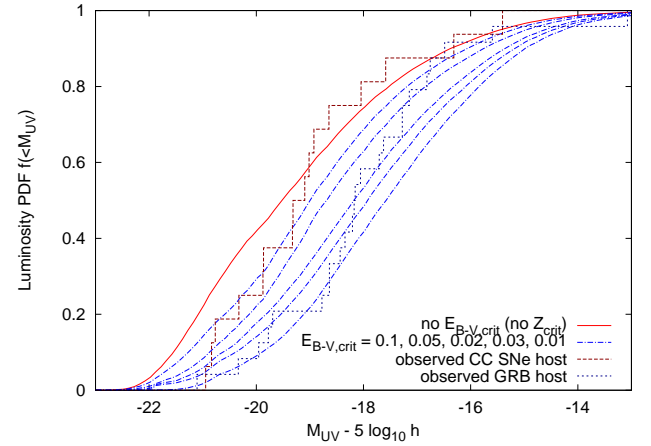

FIG. 12.— Same as Fig. 8, but here the galaxy is excluded from the sample if the average extinction value of galaxy exceeds $E_{B-V,crit}$. We use Model 0 in this figure.

In this section we discuss the possibility that the systematic faintness and the low-metallicity of the observed GRB host galaxies is caused by the observational bias against dusty host galaxies, *not* by the intrinsic nature of GRB progenitors. It is difficult to identify the GRB host galaxy without a detection of an optical afterglow, and the afterglow flux may be reduced significantly by the dust extinction effect. In fact, some GRBs have optical to X-ray afterglow spectral index $\beta_{OX} < 0.5$[6], which is smaller than the expectation from the standard external shock model of GRB afterglows (e.g., Jakobsson et al. 2004). We note that a part of the optically dark GRB could also be caused by the effects other than the dust extinction in their host galaxies, such as the attenuation by neutral hydrogen in the intergalactic medium at $z \gtrsim 6$ (e.g., Totani et al. 2006; Nagamine et al. 2008).

In order to examine the effect of dust extinction in the host galaxy (as opposed to the extinction in the immediate nearby environment of the GRB), here we exclude the galaxy from the sample of simulated host galaxies if $E_{B-V} \geq E_{B-V,crit}$,

[6] The optical to X-ray afterglow spectral index β_{OX} is defined as $f_{opt}/f_X = (\lambda_{opt}/\lambda_X)^{\beta_{OX}}$, where f_{opt} and f_X are the optical and X-ray fluxes, respectively.
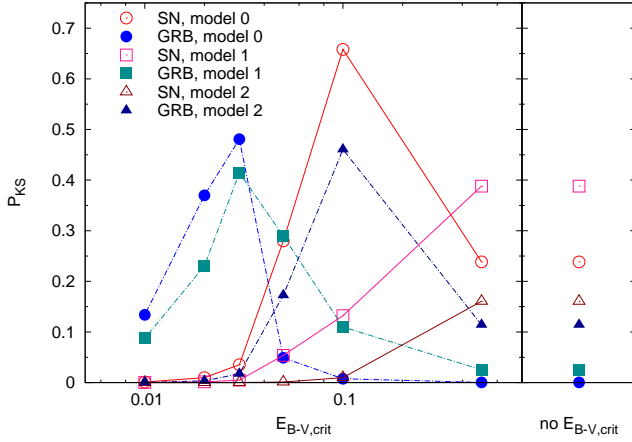
FIG. 13.— Same as Figs. 9 and 11, but here P_{KS} is plotted against $E_{B-V,\mathrm{crit}}$ instead of Z_{crit}.

FIG. 14.— Fraction of optically dark GRBs at $z = 1.0$ in our simulation (i.e., the fraction of GRB events in galaxies with $E_{B-V} > E_{B-V,\mathrm{crit}}$) as a function of $E_{B-V,\mathrm{crit}}$. The results for three different values of Z_{crit} are shown. The observed range of fractions for the GRBs at all redshifts (Cenko et al. 2009; Zheng et al. 2009) is indicated with the shade. We use Model 0 in this figure.

where E_{B-V} is the average extinction of each galaxy computed in § 2.3. The GRB event rate in each galaxy is assumed to be proportional to the SFR in the galaxy. Figure 12 shows the cumulative luminosity PDF of simulated host galaxies with various $E_{B-V,\mathrm{crit}}$. The no-$E_{B-V,\mathrm{crit}}$ case (*red solid* line) represents the luminosity PDF of GRB host galaxies when the GRB rate simply traces the SFR, and it is identical to the no-Z_{crit} case in Figure 8. The luminosity PDF of the simulated host galaxies shifts to the fainter magnitudes with smaller $E_{B-V,\mathrm{crit}}$, similarly to the Z_{crit} dependence shown in Figure 8.

Figure 13 shows the K-S probability versus $E_{B-V,\mathrm{crit}}$ for the luminosity PDF of the Model 0 galaxies given in Figure 12, together with the results of Model 1 & 2 galaxies. For Model 0 & 1, a reasonable agreement ($P_{KS} > 0.2$) between the simulated and observed distributions of the SN host galaxies is found for a wide range of critical extinction ($E_{B-V,\mathrm{crit}} \geq 0.05$), while for the GRB host galaxies the same level of agreement is achieved only when $E_{B-V,\mathrm{crit}} \leq 0.03$.

The above requirement of $E_{B-V,\mathrm{crit}} \leq 0.03$ for the GRB host galaxies of the Models 0 & 1 does not seem to agree with observations. Some follow up observations of optically dark GRBs suggest that a typical dust extinction to make a GRB optically dark is $A_V \sim 1$ (e.g., Perley et al. 2009, $E_{B-V} \sim 0.3$), which is much larger than the above requirement of $E_{B-V,\mathrm{crit}} < 0.03$. Such large values of critical extinction ($E_{B-V,\mathrm{crit}} > 0.1$) do not significantly change the luminosity PDF of simulated host galaxies. A small dust extinction such as $E_{B-V} < 0.03$ is unlikely to have a significant impact on the GRB optical afterglow observations.

For the Model 2, the agreement with the observed GRB hosts is good ($P_{KS} = 0.48$) at $E_{B-V,\mathrm{crit}} = 0.1$, however, $P_{KS} > 0.2$ is not obtained for the SN host galaxies with any values of $E_{B-V,\mathrm{crit}}$. The SFR-weighted luminosity PDF of the Model 2 galaxies are too faint to agree with the observation of SN host galaxies even in the no-$E_{B-V,\mathrm{crit}}$ case. Hence the difference of luminosity PDFs between the GRB host and SN host galaxies cannot be reproduced by the Model 2.

A caveat here is that the E_{B-V} is computed in our model assuming simplified structure of ISM in each galaxy without considering smaller scale structures such as molecular clouds. Though our model of dust extinction reproduces the observed B-band LF of field galaxies, the model may be not representative of dust extinction for lines of sight to GRBs, if small scale structures near GRBs play an important role in the extinction
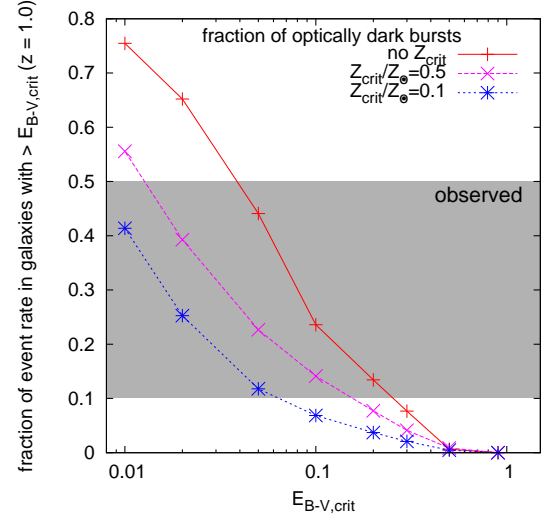
of GRB optical afterglows. Recent observations of optically dark GRBs actually suggest that the effect of dust on small scales may be important (Rol et al. 2007; Castro-Tirado et al. 2007; Perley et al. 2009; Hashimoto et al. 2010; Holland et al. 2010). If the typical extinction in lines of sight to GRBs is greater than the average extinction in its host galaxy by one order of magnitude but yet proportional to the average extinction, the luminosity PDF of GRB host galaxies possibly be reproduced by the observational bias against dusty host galaxies.

In this section, we have considered the possibility that the observational bias against dusty host galaxies is causing the systematic faintness of GRB host galaxies. However, we note that the SN observations possibly suffer more from dust extinction than the optical GRB afterglow observations. In that case, the observational bias against dusty host galaxies would make the SN host galaxy sample fainter than the GRB host galaxies, which is opposite to the observational result. Our simulation does not contradict with the observations even if the SN observations suffer from dust extinction, because the simulated luminosity PDF with $E_{B-V,\mathrm{crit}} \geq 0.1$ agrees with the SN host observations reasonably well ($P_{KS} > 0.2$) for the Model 0.

4.1.2. *Fraction of Optically Dark GRBs*

The physical nature of optically dark GRBs is also an important issue. A recent study by Cenko et al. (2009) reported that the fraction of optically dark GRBs in the entire observed GRB sample is $\sim 50\%$, while Zheng et al. (2009) found that the fraction is $\sim 10-20\%$. Note that these fractions are based on the entire GRB sample that span a wide redshift range, because it is difficult to constrain the redshift of optically dark GRBs.

In Figure 14, we show the fraction of GRB event rate in galaxies with $E_{B-V} > E_{B-V,\mathrm{crit}}$ at $z = 1.0$ in our simulation for three different values of Z_{crit}. Assuming that a GRB at $z = 1.0$ becomes optically dark when the host galaxy has $E_{B-V} \geq E_{B-V,\mathrm{crit}} = 0.3$ ($A_V \gtrsim 1$, Perley et al. 2009), our simulation predicts that the fraction of optically dark GRBs is $\lesssim 10\%$ for all cases of Z_{crit}. For the no-Z_{crit} case (*red solid* line),

the dark fraction is close to 10% for $E_{B-V,\mathrm{crit}} = 0.3$, and is almost consistent with the observational result of Zheng et al. (2009). However, if $Z_{\mathrm{crit}} < 0.5\,Z_\odot$ (as suggested in § 3), our simulation predicts that the fraction of optically dark GRBs is $< 5\%$ for $E_{B-V,\mathrm{crit}} = 0.3$, which is much smaller than the observed fraction.

The small fraction of optically dark GRBs in our simulation compared to the observations can be explained in two different ways. The first possibility is that the optically dark GRBs mainly suffer from the absorption in the optical wavelength due to dust associated with small scale structures, not from the galaxy scale dust as modeled in § 2.3. The second possibility is that many of the observed optically dark GRBs originate at different redshifts other than $z \sim 1.0$, although the redshift distribution of GRBs with known redshifts that are typically optically non-dark, peaks at $z \sim 1.0$. The fractional contribution of dusty galaxies to the cosmic SFR would be different at different redshifts. Furthermore, the afterglow of a GRB at $z \gtrsim 6$ would be attenuated by neutral intergalactic medium in the observer-frame optical bands.

It is unclear which of the above two scenarios might be correct at this point. Some observational studies (Castro-Tirado et al. 2007; Perley et al. 2009; Holland et al. 2010) find that the host galaxies of optically dark GRBs have bluer colors than those expected from the dust reddening estimated from the afterglow spectra. On the other hand, the host galaxies that is globally dusty are also found for several optically dark GRBs (Levesque et al. 2010; Hashimoto et al. 2010).

4.2. Comparison with Previous Works

Several studies have been performed to interpret the observed luminosity PDFs of GRB and SN host galaxies. In this section we compare our study with previous results.

Wolf & Podsiadlowski (2007) is one of the important studies in this context. They reproduced the luminosity PDFs of the observed GRB and SN host galaxies based on the empirical relations of galaxy properties at $z \sim 0.7$, such as the luminosity-metallicity relationship. In their study, the model in which the GRBs occur in high metallicity regions ($Z \sim Z_\odot$) reproduces the luminosity PDF of GRB host galaxy the best, and the models which requires GRBs to occur only in sub-solar metallicity regions do not reproduce the observations. They assumed a power-law relation for the luminosity-metallicity relation of galaxies following Kobulnicky & Kewley (2004). However this relationship is not well constrained by current observations at redshifts of our concern, and in the work of Kobulnicky & Kewley (2004), different fitting methods gave different set of best fit parameters for a set of observed data, suggesting large uncertainties in the fit. We also note that the results probably depend on the assumed dispersion around the power-law luminosity-metallicity relation.

Kocevski et al. (2009) studied the stellar mass PDF of GRB host galaxies in a similar way to that of Wolf & Podsiadlowski (2007) and argued for $Z_{\mathrm{crit}} > 0.5\,Z_\odot$. The mass-metallicity relationship of galaxies are better understood than the luminosity-metallicity relation (Tremonti et al. 2004; Savaglio et al. 2005). However, it is difficult to understand the selection effects of the currently available samples of GRB host galaxies with known $M_\star$. Kocevski et al. (2009) discussed the observed samples of GRB host galaxies with known $M_\star$ collected by Castro Cerón et al. (2008) and Savaglio et al. (2009). Both of the samples were col-

lected from publicly available data of GRB host observations. Castro Cerón et al. (2008) collected all GRB host galaxies with rest-frame K-band data including upper limits, while Savaglio et al. (2009) selected their sample requiring multi-band detection of the host galaxies. The observations of GRB host galaxies in the samples are originally done by various groups with differing instrument, and hence the selection effects in the samples are hardly understood. We also note that the constraints on the stellar masses for some of the GRB host galaxies in their sample are not accurate enough to quantitatively discuss the low-metallicity preference.

The approaches of Wolf & Podsiadlowski (2007) and Kocevski et al. (2009) are entirely based on the empirical relations, and are fundamentally different from our approach based on numerical simulations. As discussed above, one difficulty in studying the luminosity PDFs of GRB/SN host galaxies is that properties of galaxies are not observationally well understood at redshifts where the observed sample is available. Numerical simulation approach is powerful in this context, because it gives properties of galaxies such as luminosity, metallicity, and SFR without assuming uncertain relations between them.

Some numerical studies have investigated the luminosity of GRB host galaxies (Nuza et al. 2007; Lapi et al. 2008; Campisi et al. 2009). However, quantitative comparisons of the predicted luminosity PDF of GRB host galaxies and the observed luminosity PDFs have not been performed in these studies. Nuza et al. (2007) did not reproduce the luminosity PDFs of both GRB and SN hosts, presumably owing to the small box size of their simulation ($10h^{-1}\,\mathrm{Mpc}$). Lapi et al. (2008) and Campisi et al. (2009) have shown that the fainter galaxies have systematically lower metallicities in their models. However, in Lapi et al. (2008) and Campisi et al. (2009), the luminosity PDFs are calculated simply by selecting galaxies that contain young low-metallicity stars without taking the difference of GRB rate among galaxies into account, therefore the predicted luminosity PDFs cannot be directly compared with the observations of GRB host galaxies.

In this context, our present work is unique in the sense that it can quantitatively reproduce the observations of both GRB and SN host galaxies using a self-consistent cosmological hydrodynamic simulations of galaxy formation. This has been enabled by applying a widely used GRB rate model to our cosmological simulations with large box sizes, which can properly compute the properties of galaxies at $z \sim 1$.

5. CONCLUSIONS

Using cosmological SPH simulations, we have examined the relation between the metallicity dependence of GRBs and the luminosity PDF of GRB host galaxies. Our results suggest that the observed difference in the UV luminosity PDFs of GRB/SN host galaxies can be explained by the low-metallicity preference of GRBs.

We find that in our simulation, the luminosity PDF of GRB host galaxies agree with the observed one when $Z_{\mathrm{crit}} < 0.5\,Z_\odot$, while the observed luminosity PDF of SN host galaxies can be reproduced without a metallicity dependence of SN rate. The suggested value of Z_{crit} for the GRBs by our study is consistent with the suggestion from stellar evolution models (Yoon & Langer 2005; Woosley & Heger 2006), contrary to the results of previous studies (Wolf & Podsiadlowski 2007; Kocevski et al. 2009). Though our simulation suffers from the seeming overprediction of the UV luminosity function at $z = 1$ at the bright end, we have explicitly demonstrated that the

quantitative agreement between the simulated and observed luminosity PDFs is not a product of this seeming overestimate of the UV-bright galaxies in our simulation. However, we should be cautious about our results when $Z_{crit} < 0.1 Z_\odot$, since they may be affected by the resolution limit of our simulation.

We have also discussed the effect of observational bias against the host galaxies of optically dark GRB on the luminosity PDFs. The dust bias causes a shift of luminosity PDFs toward fainter magnitudes, similarly to the effect of the low-metallicity preference of GRBs. However, to obtain an acceptable fit to the observed luminosity PDF of GRB host galaxies, we had to assume that an optical afterglow becomes significantly faint when $E_{B-V} \sim 0.03$ in the host galaxy. Such a small extinction is unlikely to cause a significant effect for the optical follow-up observations of GRBs, and therefore it would be difficult to explain the observed luminosity PDFs of GRB and SN host galaxies only by the overall dust bias of the host galaxies. Nevertheless it is possible that our simplified model of dust extinction is not sufficient to reproduce the dust extinction of GRB optical afterglows.

Assuming that a GRB becomes optically dark when the extinction of its host galaxy is $E_{B-V} \gtrsim 0.3$ as suggested by the observation of Perley et al. (2009), our simulation predicts that the fraction of optically dark GRBs at $z = 1.0$ is $< 5\%$ for $Z_{crit} \leq 0.5 Z_\odot$. This fraction is significantly smaller than what is suggested by the observations of GRBs at all redshifts (Perley et al. 2009; Zheng et al. 2009). This is probably because we did not consider the dust extinction effect on small scales at the GRB site. It is also possible that the GRBs at redshifts other than $z \sim 1$ are important in determining the fraction. We plan to address the effect of small scale dust in the future using higher resolution simulations.

REFERENCES

Bohlin, R. C., Savage, B. D., & Drake, J. F. 1978, ApJ, 224, 132
Bouchet, P., Lequeux, J., Maurice, E., Prevot, L., & Prevot-Burnichon, M. L. 1985, A&A, 149, 330
Bruzual, G., & Charlot, S. 2003, MNRAS, 344, 1000
Calzetti, D. 1997, AJ, 113, 162
Campisi, M. A., De Lucia, G., Li, L., Mao, S., & Kang, X. 2009, MNRAS, 400, 1613
Castro Cerón, J. M., Michałowski, M. J., Hjorth, J., Malesani, D., Gorosabel, J., Watson, D., & Fynbo, J. P. U. 2008, arXiv:0803.2235
Castro-Tirado, A. J., et al. 2007, A&A, 475, 101
Cenko, S. B., et al. 2009, ApJ, 693, 1484
Choi, J., & Nagamine, K. 2009, MNRAS, 393, 1595
—. 2010, MNRAS, 407, 1464
Dahlen, T., Mobasher, B., Dickinson, M., Ferguson, H. C., Giavalisco, M., Kretchmer, C., & Ravindranath, S. 2007, ApJ, 654, 172
Faber, S. M., et al. 2007, ApJ, 665, 265
Fitzpatrick, E. L. 1985, ApJS, 59, 77
Fruchter, A. S., et al. 2006, Nature, 441, 463
Fynbo, J. P. U., et al. 2002, A&A, 388, 425
—. 2003, A&A, 406, L63
Haardt, F., & Madau, P. 1996, ApJ, 461, 20
Hashimoto, T., et al. 2010, arXiv:1003.3717
Hernquist, L. 1990, ApJ, 356, 359
Hjorth, J., et al. 2003, Nature, 423, 847
Holland, S. T., et al. 2010, ApJ, 717, 223
Jakobsson, P., Hjorth, J., Fynbo, J. P. U., Watson, D., Pedersen, K., Björnsson, G., & Gorosabel, J. 2004, ApJ, 617, L21
Jakobsson, P., et al. 2005, MNRAS, 362, 245
Kistler, M. D., Yüksel, H., Beacom, J. F., Hopkins, A. M., & Wyithe, J. S. B. 2009, ApJ, 705, L104
Kobulnicky, H. A., & Kewley, L. J. 2004, ApJ, 617, 240
Kocevski, D., West, A. A., & Modjaz, M. 2009, ApJ, 702, 377
Komatsu, E., et al. 2009, ApJS, 180, 330
—. 2010, arXiv:1001.4538
Lapi, A., Kawakatu, N., Bosnjak, Z., Celotti, A., Bressan, A., Granato, G. L., & Danese, L. 2008, MNRAS, 386, 608

Larsson, J., Levan, A. J., Davies, M. B., & Fruchter, A. S. 2007, MNRAS, 376, 1285
Le Floc'h, E., et al. 2003, A&A, 400, 499
Levesque, E. M., Kewley, L. J., Graham, J. F., & Fruchter, A. S. 2010, ApJ, 712, L26
MacFadyen, A. I., & Woosley, S. E. 1999, ApJ, 524, 262
Modjaz, M., et al. 2008, AJ, 135, 1136
Nagamine, K., Zhang, B., & Hernquist, L. 2008, ApJ, 686, L57
Niino, Y., Totani, T., & Kobayashi, M. A. R. 2009, ApJ, 707, 1634
Nuza, S. E., Tissera, P. B., Pellizza, L. J., Lambas, D. G., Scannapieco, C., & de Rossi, M. E. 2007, MNRAS, 375, 665
Pérez-Montero, E., et al. 2009, A&A, 495, 73
Perley, D. A., et al. 2009, AJ, 138, 1690
Rol, E., et al. 2007, ApJ, 669, 1098
Savaglio, S., Glazebrook, K., & Le Borgne, D. 2009, ApJ, 691, 182
Savaglio, S., et al. 2005, ApJ, 635, 260
Springel, V. 2005, MNRAS, 364, 1105
Springel, V., & Hernquist, L. 2002, MNRAS, 333, 649
—. 2003, MNRAS, 339, 289
Springel, V., White, S. D. M., Tormen, G., & Kauffmann, G. 2001, MNRAS, 328, 726
Stanek, K. Z., et al. 2003, ApJ, 591, L17
—. 2006, Acta Astronomica, 56, 333
Svensson, K. M., Levan, A. J., Tanvir, N. R., Fruchter, A. S., & Strolger, L. 2010, MNRAS, 405, 57
Totani, T., Kawai, N., Kosugi, G., Aoki, K., Yamada, T., Iye, M., Ohta, K., & Hattori, T. 2006, PASJ, 58, 485
Tremonti, C. A., et al. 2004, ApJ, 613, 898
Tumlinson, J., et al. 2002, ApJ, 566, 857
Wolf, C., & Podsiadlowski, P. 2007, MNRAS, 375, 1049
Woosley, S. E., & Heger, A. 2006, ApJ, 637, 914
Yoon, S., & Langer, N. 2005, A&A, 443, 643
Zhang, B., et al. 2009, ApJ, 703, 1696
Zheng, W., Deng, J., & Wang, J. 2009, Research in Astronomy and Astrophysics, 9, 1103